Available online at website: https://journal.bcrec.id/index.php/bcrec

Bulletin of Chemical Reaction Engineering & Catalysis, 20 (4) 2025, 736-749

Original Research Article

Missing Linker Defects in Heterometallic (Zn/Cd)-MOF-5: A First-Principles Study of Structural Properties and Gas Interaction

Fajar Inggit Pambudi*, Eko Sri Kunarti, Robby Noor Cahyono, Nabila Nur Agusti

Department of Chemistry, Faculty of Mathematics and Natural Sciences, Universitas Gadjah Mada, Sekip Utara, Bulaksumur, Yogyakarta 55281, Indonesia.

Received: 5th August 2025; Revised: 15th October 2025; Accepted: 15th October 2025
Available online: 23th October 2025; Published regularly: December 2025

Abstract

The defect structures in multicomponent metal-organic frameworks (MOFs), specifically mixed-metal (Zn/Cd)-MOF-5, were investigated by examining the removal of a benzenedicarboxylate (bdc^{2-}) linker. The defect formation, induced by the reaction with water, was studied, and the reaction energy was calculated to be relatively low, ranging from 0.24 eV to 0.60 eV. The removal of a bdc^{2-} linker is energetically favourable when it is initially coordinated to both Zn^{2+} and Cd^{2+} ions. The electronic properties of defective (Zn/Cd)-MOF-5 were analyzed in terms of bandgap energy and density of states profile. The removal of the bdc^{2-} linker slightly reduced the bandgap energy and affected the electronic states of both carbon and oxygen atoms. To evaluate the impact of defects, interactions with various gas molecules, including H_2O, CO_2, CO, H_2S, and NO_2, were studied. The defective (Zn/Cd)-MOF-5 showed a strong preference for H_2O molecules, while CO_2 exhibited the lowest binding preference among the gases studied.

Keywords: metal-organic frameworks; MOF; defect; mixed metals; gas adsorption; DFT

How to Cite: Pambudi, F. I., Kunarti, E. S., Cahyono, R. N., Agusti, N. N. (2025). Missing Linker Defects in Heterometallic (Zn/Cd)-MOF-5: A First-Principles Study of Structural Properties and Gas Interaction. *Bulletin of Chemical Reaction Engineering & Catalysis*, 20 (4), 736-749. (doi: 10.9767/bcrec.20464)

Permalink/DOI: https://doi.org/10.9767/bcrec.20464

1. Introduction

Metal-organic frameworks (MOFs) belong to the extensive family of coordination polymers, where interactions between metal clusters or metal oxides and organic linkers dictate the formation of diverse frameworks [1,2]. The intrinsic properties of MOFs are crucial for designing nanoporous materials for targeted applications. Various synthetic approaches, such as incorporating multiple components into a pristine MOF or introducing structural defects, have been explored [3,4]. Consequently, MOFs have been intensively studied for applications including gas adsorption, gas separation, catalysis, and drug delivery [5–11].

The diversity in MOF synthesis allows for the creation of multi-component MOFs, where a single MOF structure may incorporate multiple types of metal ions or organic linkers [12,13]. This approach can provide additional binding sites for guest molecules [14]. Several advantages of multi-component MOFs have been reported, such as increased stability and improved electronic properties compared to single-component MOFs. Specifically, mixed-metal MOFs, which contain multiple types of metal ions, offer enhanced opportunities to modify electronic properties and provide additional active sites for gas adsorption and catalysis [15–17].

Mixed-metal MOFs have been reported for various well-known MOFs, such as: UiO-66, ZIFs, and MILs [18–21]. The presence of different metal ions can alter the coordination behavior of the metal cluster or node due to different electronic

* Corresponding Author.
Email: fajar.inggit@ugm.ac.id (F.I. Pambudi)

configuration [22]. Therefore, the interaction between metal ions and organic linkers may vary in bond length, potentially distorting the structure. Additionally, the oxidation states of metal ions affect bonding, leading to either saturated or unsaturated metal sites. Therefore, incorporating specific metal ions within the MOF structure can be tailored for targeted applications, where these ions act as active sites while maintaining the chemical and physical stability of the pristine MOFs.

To enhance the activity of MOF materials, defects are typically introduced during synthesis using various competing agents for the original ligands or through post-synthetic reactions such as etching [23–26]. Various types of defects, including missing linkers, missing metals, and structural defects like rotational defects, are well-studied in MOF materials [27,28]. The presence of defects provides additional binding sites due to possible unsaturated metal coordination in missing linker defects or an extra pore dimension due to missing metal cluster, which may be beneficial for guest molecule interactions [29–33]. Defect formation can also occur in multicomponent MOFs, especially mixed-metal MOFs, by inducing missing linker approaches. In this case, defective mixed-metal MOFs may offer unsaturated metal sites from different types of metal ions present in the mixed-metal structure.

Designing MOF materials containing defects is crucial for applications in gas separation and capture, particularly for CO_2. The increase in CO_2 levels in the atmosphere due to industrial activities is a concern for both human health and the environment [34]. Additionally, various chemical industries release different gas molecules such as CO, H_2S, and NO_2, especially from flue gases. Besides these gases, water vapor may also be released from flue gas as part of a mixture with other hazardous gases. Therefore, the use of defective mixed-metal MOFs is essential for gas separation and capture due to the presence of unsaturated metal sites from various metal ions.

This first-principles computational study investigates the structural and gas adsorption properties of defective, mixed-metal (Zn/Cd)-MOF-5, presenting a novel approach by focusing on the synergistic effects of heterometallic nodes and missing linker defects. The principal novelty lies in providing the first detailed analysis of how Zn^{2+} and Cd^{2+} ions cooperatively stabilize defects and modulate electronic properties, offering a comprehensive evaluation of their combined impact on flue gas molecule selectivity. The MOF-5 framework was strategically selected for this foundational study over more complex systems like UiO-66 or MIL-101 due to its prototypical and well-defined paddle-wheel [Zn_4O] cluster, which provides a simple, highly symmetric environment ideal for isolating the effects of metal substitution. The isoelectronic with distinct nature of Zn^{2+} and Cd^{2+} (differing in ionic radius and electronegativity) allows for an investigation into how these fundamental properties influence lattice strain, defect formation, and resultant gas interaction. Although cadmium is used here as a computational model due to its favorable comparative properties with zinc, its known toxicity limits its practical application. The insights gained from this study, however, are intended to establish general design principles for mixed-metal MOFs that can be applied to more environmentally benign metal pairs. By employing periodic density functional theory for the defect study and cluster models for gas interaction energetics, this work establishes a foundational understanding for the targeted design of multicomponent defective MOFs for gas separation applications.

2. Computational Methods

The initial structure of MOF-5 was derived from experimental X-ray diffraction data, with lattice parameters of $a = b = c = 25.6690$ Å [35]. The primitive cubic structure was used for the calculation. Due to the large number of atoms in a unit cell, all calculations were performed on a single unit cell of MOF-5. The initial structure was first geometry-optimized to obtain the equilibrium structure of (Zn)-MOF-5 (Figure 1a). From this optimized structure, the mixed-metal (Zn/Cd)-MOF-5 structures, labelled as 1MM and 2MM, were developed, as shown in Figures 1b and 1c, respectively.

Defect structures were generated from the optimized mixed-metal Zn/Cd-MOF-5 structure to model defects caused by missing organic linkers. Nine possible configurations of defective Zn/Cd-MOF-5 were modelled based on the 1MM and 2MM structures. From the optimized mixed-metal (Zn/Cd)-MOF-5 (1MM) (Figure 1b), four missing linker structures were annotated as structures A, B, C, and D. Additionally, using the optimized structure in Figure 1c (2MM), five different missing linkers were modelled, annotated as structures E, F, G, H, and I. The differences between these missing linker structures arise from the arrangement of capping agents, which include hydroxide (OH-) and water molecules (H2O).

DFT calculations were performed with the Quickstep module implemented in the CP2K code [36]. All structures were optimized by relaxing both the atomic coordinates and the unit cell size while the angle between unit cell axes is kept fix. The calculation was performed using Perdew-Becke-Ernzerhof (PBE) with the addition of Grimme D3 correction to account for possible weak interactions. The basis set of TZVP-

MOLOPT was used for C, O and H atoms while DZVP-MOLOPT was used for Cd and Zn. The Goedecker-Teter-Hutter (GTH) pseudopotential was used to treat the core electrons. An energy cutoff of 600 Ry was used in all calculations. The SCF convergence was set to 1×10^{-6} Hartree. The optimization was completed when the maximum force is less than 4.5×10^{-4} Ha.Bohr^{-1}. All the DFT calculations were conducted by considering the spin contribution affect.

Single point energy calculation was performed to obtain the reaction energy of defect formation as well as the electronic properties. The reaction energy ($E_{reaction}$) for missing bdc^{2-} linker was calculated according to the equation (1).

$$E_{reaction} = (E_{defect} + E_{ligand}) - (E_{MOF} + E_{water}) \quad (1)$$

E_{defect} is the defective energy of Zn/Cd-MOF-5 due to missing bdc^{2-} ligand, E_{ligand} is energy of H2bdc

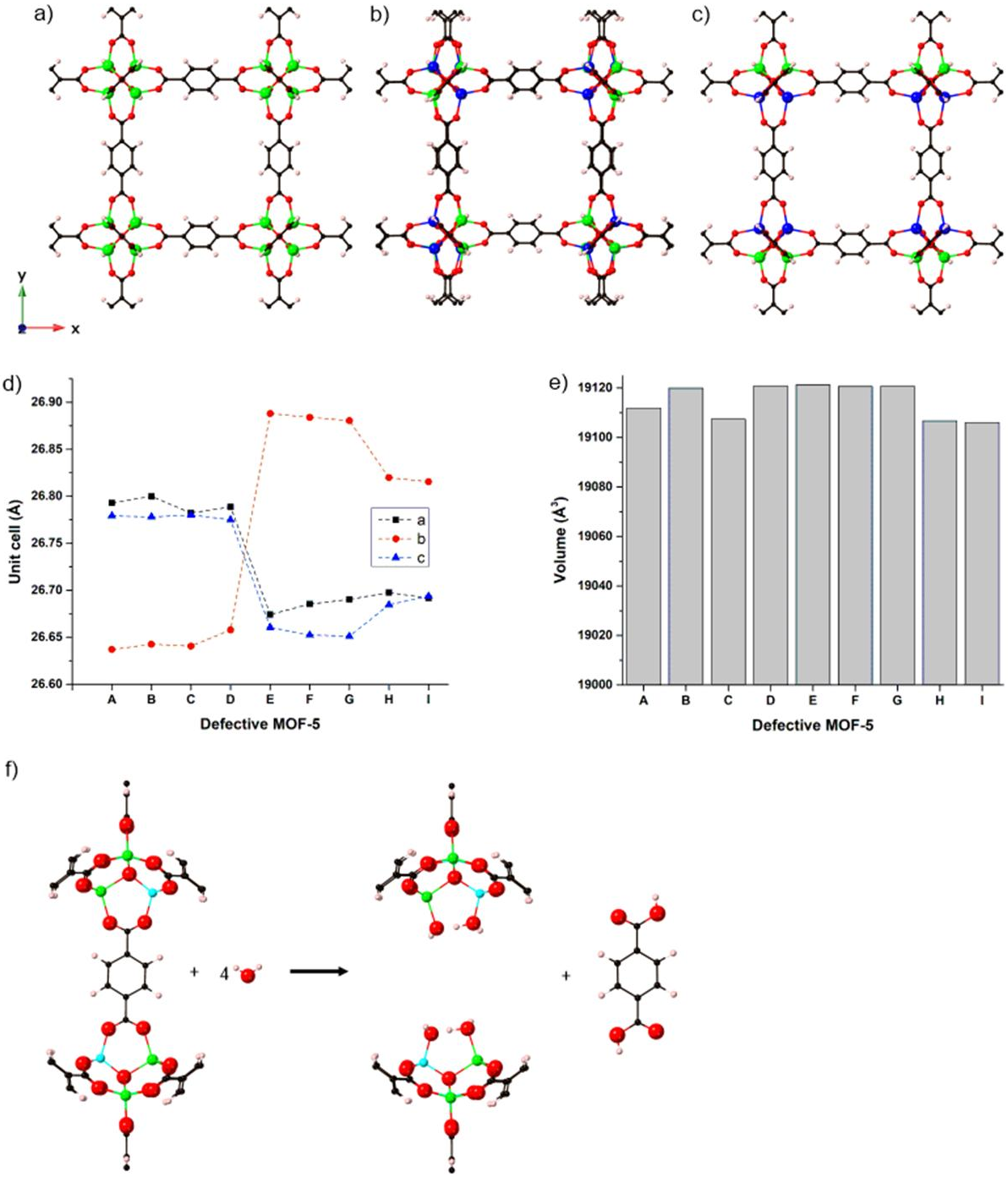

Figure 1. The optimised structure of MOF-5 (a), and mixed-metal (Zn/Cd)-MOF-5 of 1MM (b) and 2MM (c). The unit cell parameter (d) and volume (e) of defective (Zn/Cd)-MOF-5 are also shown. The illustration of reaction between mixed-metal (Zn/Cd)-MOF-5 and water to give missing linker defect is shown in image (f). Zn, Cd, C, O and H are coloured with green, blue, black, red and pink colour, respectively.

ligand, E_{MOF} is the energy of pristine (Zn/Cd)-MOF-5, and E_{water} is energy of water molecule. The missing linker defect is assumed due to the reaction between mixed-metal (Zn/Cd)-MOF-5 and water molecules as illustrated in Figure 1f.

The interaction between defective (Zn/Cd)-MOF-5 and gas molecules was conducted by using a cluster model of defective (Zn/Cd)-MOF-5. Two cluster models were chosen by showing unsaturated metal sites of Zn^{2+} and Cd^{2+} after removing a bdc^{2-} linker. The binding energy (E) was calculated with equation (2).

$$E = E_{(MOF+gas)} - E_{(MOF)} - E_{(gas)} \quad (2)$$

where the $E_{(MOF+gas)}$ is the electronic energy of the host-guest structure, while $E_{(MOF)}$ and $E_{(gas)}$ are the electronic energy of the defective (Zn/Cd)-MOF-5 and the gas molecule, respectively. The binding energy was calculated by considering the basis set superposition error using the Counterpoise method. The DFT calculation of the cluster model was performed with ORCA5.0 software utilising the B3LYP method, basis set of def2-TZVP for all atoms and VERYTIGHTSCF criteria [37]. Dispersion correction with Becke-Johnson damping (D3BJ) was utilised during all calculations.

3. Results and Discussion

3.1 Structure of Pristine and Mixed-metal MOF-5

The structure of MOF-5 was calculated using the periodic DFT method, yielding unit cell parameters of $a = b = c = 26.1193$ Å and a unit cell volume of 17819.154 Å3. These values are reasonably close to the experimental unit cell dimensions of $a = b = c = 25.6690$ Å [35]. All DFT calculations adhered strictly to convergence criteria, ensuring the maximum force on each atom was below 4.5×10^{-4} Ha.Bohr^{-1}. The bandgap energy of pristine MOF-5 was calculated to be 3.63 eV, which aligns well with the reported values of 3.4 - 4.0 eV [38].

The structure of mixed-metal Zn/Cd-MOF-5 was derived from pristine MOF-5, as shown in Figure 1. This mixed-metal structure was developed by positioning Zn^{2+} and Cd^{2+} ions in a 1:1 ratio, resulting in 16 Zn^{2+} ions and 16 Cd^{2+} ions, creating a variety of missing linkers for the defect structure. The mixed-metal Zn/Cd-MOF-5 (1MM) in Figure 1b exhibits unit cell parameters of $a = 26.6803$ Å, $b = 26.8478$ Å, and $c = 26.6802$ Å, which are on average 2.35% larger than those of pristine MOF-5. A similar increase was observed in the second mixed-metal configuration of 2MM (Figure 1c), with unit cell dimensions of $a = 26.7637$ Å, $b = 26.6678$ Å, and $c = 26.7658$ Å, averaging 2.34% larger than pristine MOF-5. This expansion is expected due to the slightly larger ionic radius of Cd^{2+} compared to Zn^{2+}, resulting in a slight unit cell expansion in the mixed-metal MOF-5.

The reaction energy is calculated based on the difference between the electronic energy of the product which is the defective MOF-5 and the reactant which is the pristine mixed-metal (Zn/Cd)-MOF-5 as illustrated in Figure 1f. The optimised structure of mixed-metal MOF-5 was used to develop defective mixed-metal MOF-5 due to missing linkers. The defect structure of missing linker (Zn/Cd)-MOF-5 was generated due to the interaction with water molecules. Therefore, at the defect sites, the capping agent is derived from both water molecule and hydroxide to compensate the overall neutral charge of the defective (Zn/Cd)-MOF-5. In this case, the position of capping H2O molecule and hydroxide (OH-) is alternated to give 9 possible structures of A, B, C, D, E, F, G, H and I. The defective (Zn/Cd)-MOF-5 indicates diverse unit cell dimension relative to the pristine MOF-5 as shown in Figure 1d. The structure of A, B, C and D provide similar behaviour where a- and c-lattice direction show relatively similar value. However, the b-lattice dimension has lower unit cell dimension due to the location of defect in line with the b-lattice direction. The same observation also occurs for the E, F, G, H and I structure where the b-lattice dimension diverges in comparison with the a-, and c-lattice dimension.

The reaction energy has been calculated to range between 0.24 eV and 0.60 eV, suggesting that the formation of missing linker defects is relatively easy in the presence of water (Figure 2). In Figures 2a-d, the defect structures are based on the 1MM structure, with alternating positions of H2O and OH-. The reaction energy range is relatively narrow, between 0.24 and 0.33 eV, indicating that the capping agents H2O and OH- can attach to either Cd^{2+} or Zn^{2+}. However, the distance between the oxygen atoms of H_2O or OH- and the metal ions differs. The average distance to Zn^{2+} is 1.987 Å, while the average distance to Cd^{2+} is 2.183 Å across all nine structures shown in Figure 2.

The missing linker defect structures E, F, G, H, and I are derived from the 2MM structure. However, structures H and I have a different configuration where the bdc^{2-} linker is initially attached to all Cd^{2+} ions. The reaction energies for structures E, F, and G are very similar, ranging between 0.35 and 0.36 eV. The location of capping agents does not significantly affect the structural stability. Slight differences in reaction energy are observed for structures H and I, with values of 0.58 and 0.60 eV, respectively. This difference is due to the initial attachment of the bdc^{2-} linker to Cd^{2+} ions. This observation suggests that the initial attachment of the bdc^{2-} ligand plays a

crucial role in the formation of missing linker defects. The bdc^{2-} linker is more easily removed when it initially bonds to both Cd^{2+} and Zn^{2+}. However, when the bdc^{2-} linker bonds only to Cd^{2+} ions, the reaction energy is higher, making it more difficult to remove the linker from the MOF structure.

The calculated reaction energies for the formation of a missing linker defect in (Zn/Cd)-MOF-5 range from 0.24 eV to 0.60 eV (23.1 to 57.9 kJ/mol). While direct experimental measurements of these energies are challenging, our computed values can be contextualized with defect studies in other MOF systems. For instance, in a mixed-metal Zn/Cd-ZIF-8 framework, the energy cost associated with the removal of a metal ion was found to be lower for Cd^{2+} than for Zn^{2+}, indicating weaker Cd–N bonding compared to Zn–N [39]. This provides a valuable parallel to this work; although this study focuses on linker removal rather than metal removal, the inherent difference in metal-linker bond strength (Zn–O vs. Cd–O) is a consistent factor influencing defect stability in mixed-metal systems. In our case, the higher reaction energies for structures H and I (0.58 and 0.60 eV), where the removed linker was initially bound exclusively to Cd^{2+} ions, suggest that disrupting the Cd–O bond in this specific coordination environment requires more energy, highlighting the complex interplay between local metal coordination and defect thermodynamics.

The presence of capping agents acts as charge-balancing species for the entire structure. According to the reaction energy, the location of either H_2O or OH^- may attach to Cd^{2+} or Zn^{2+} ions without significantly affecting the reaction energy. Since H_2O and OH^- are in close proximity, there is bond elongation of the O–H bond in the H_2O capping agent. In Figure 3, the location of the water molecule is highlighted with black circles. The hydrogen atom of the H_2O molecule, which is close to the OH^- capping, is slightly distorted from the H_2O molecule. The O–H distance is calculated to be 1.140 Å for structure A, for example. This O–H bond distance is slightly longer than the O–H bond distance in a water molecule, which is about 0.971 Å for structure A. The elongation of the O–H bond in the H_2O capping is due to possible intermolecular interaction with the OH- capping agent, potentially forming hydrogen bonds. Therefore, there is a possibility of deprotonation of the H_2O molecule as the capping agent.

The critical role of capping agents in stabilizing defects is universally observed. A study on defective MOF-801 demonstrated that the defect formation energy is highly sensitive to the nature of the capping species, with energies ranging from highly unfavourable (+256.2 kJ/mol for OH^- capping) to thermodynamically spontaneous (-91.3 kJ/mol for $Cl^- + H_2O$ capping) [40]. Our models, which employ a combination of H_2O and OH^- as capping agents, yield defect energies in a moderate, accessible range (23.1–57.9 kJ/mol or 0.24 – 0.60 eV). This aligns with the MOF-801 results, confirming that the specific charge-balancing species present during defect formation (in this case, derived from aqueous conditions) are crucial for determining the thermodynamic feasibility of defect incorporation.

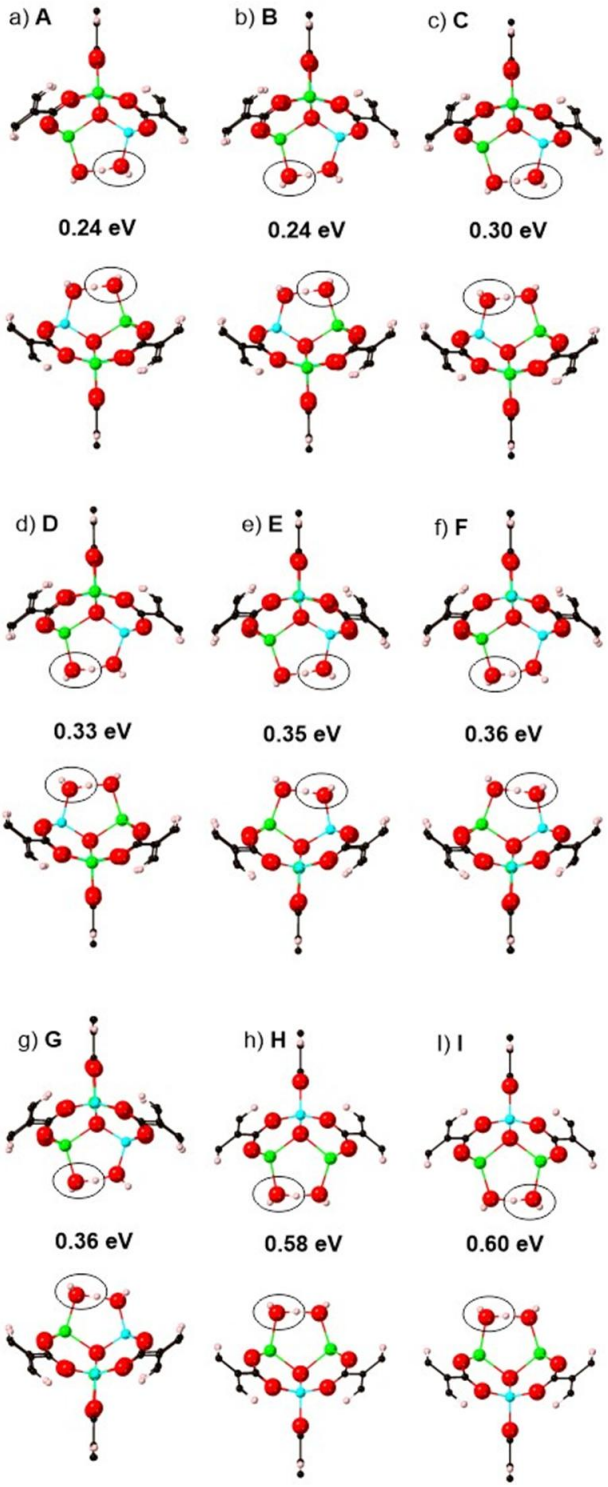

Figure 2. The optimised structures and reaction energy of missing linker defect (Zn/Cd)-MOF-5.

3.2 Electronic Properties of Defective Mixed-Metal MOF-5

The electronic band structure of MOFs is a critical determinant of their functionality in applications such as photocatalysis and chemical sensing. Pristine MOF-5 is a wide bandgap semiconductor of 3.63 eV from our calculation which is aligning with reported values of 3.4 - 4.0 eV [38], which restricts its photoactivity to the UV region of the electromagnetic spectrum and limits its practical use under solar illumination. In this study, the introduction of a second metal (Cd) into the MOF-5 framework resulted in only a minimal reduction of the bandgap, with the mixed-metal 1MM and 2MM structures exhibiting bandgaps of 3.61 eV and 3.59 eV, respectively. While this change is small, it signifies a crucial electronic perturbation at the metal-oxide node due to the different electronegativity and orbital energy of Cd^{2+} compared to Zn^{2+}. This confirms that heterometallic incorporation can fine-tune the electronic landscape of the MOF, even within an isostructural framework.

A more pronounced and consistent trend is observed upon the introduction of missing linker defects. As listed in Table 1, all nine defective structures exhibit a further reduction in bandgap, ranging from 3.55 eV to 3.58 eV. Although these reductions may appear modest (a narrowing of ~ 0.03-0.06 eV from the mixed-metal parent structures), their significance is also pronounced in photocatalysis and chemical sensing. For photocatalytic applications, even a small reduction in bandgap energy can have a substantial impact on efficiency. A shift from 3.61 eV to 3.55 eV corresponds to a change in the absorption edge from ~343 nm to ~349 nm. More importantly than this slight redshift, the defect states may significantly improve the separation and lifetime of photogenerated electron-hole pairs.

Table 1. The bandgap energy of pristine mixed-metal(Zn2/Cd)-MOF-5 and missing linker defect in (ZnCd)-MOF-5.

MOFs	Bandgap energy (eV)
1MM	3.61
2MM	3.59
A	3.57
B	3.56
C	3.57
D	3.55
E	3.55
F	3.58
G	3.58
H	3.55
I	3.55

The electronic states of missing linker defects provide valuable information regarding bandgap energy, hybridization, and the contribution from each atomic orbital in the structure. As shown in Figure 3, the partial density of states (DOS) for hydrogen, which is dominated by the s orbital, has a small contribution to the overall electronic states compared to other atoms. The electronic state density of hydrogen indicates interaction with carbon, as evidenced by the similar patterns or possible overlapping states, which is expected for the covalent C–H bond in the bdc^{2-} linker. The most dominant contributions to the electronic structure come from carbon and oxygen in the bdc^{2-} linker at the edges of the valence and conduction bands. At the edge of the valence band, the electronic states of oxygen are much broader than those of carbon, as the oxygen atom is connected to the metal ions (Cd^{2+} or Zn^{2+}) as well as being part of the bdc^{2-} linker.

The contribution of metal ions, either Cd^{2+} or Zn^{2+}, is mostly below the edge of the valence band. The electronic states of Cd^{2+} and Zn^{2+} are particularly high at lower energies, specifically below -4 eV. This behaviour corresponds to the electronic states of oxygen at energies less than -4 eV, indicating possible hybridization due to the interaction between metal ions and the oxygen of bdc^{2-} ligand (Cd^{2+}–O and Zn^{2+}–O). At the edge of the valence band, the contribution of metal ions to the decrease in bandgap energy is minimal, as there is no significant difference in the electronic states. The decrease in bandgap energy due to the missing linker can be explained by the slight differences in the electronic states of carbon at the edge of the valence band. In the 1MM and 2MM structures, the electronic states of carbon at the valence band are slightly higher in energy compared to the electronic states of carbon in the missing linker defects. This is expected since the absence of the bdc^{2-} linker affects the electronic states of primarily carbon and oxygen atoms.

3.3 Interaction of Defective Mixed-Metal MOFs with Gas Molecule

To investigate the interaction between defective mixed-metal (Zn/Cd)-MOF-5 and gas molecules, we utilized a cluster model derived from the optimized structures of mixed-metal MOF-5, specifically the 1MM and 2MM configurations (see Figure 1). The capping agents OH^- and H_2O were removed to simulate the activated form of defective (Zn/Cd)-MOF-5, exposing unsaturated Zn^{2+} and Cd^{2+} ions as active sites. The interactions between defective (Zn/Cd)-MOF-5 (1MM) and various gas molecules were examined, as depicted in Figure 4. Initially, the gas molecules were positioned centrally between the Zn^{2+} and Cd^{2+} active sites. Calculations revealed that the interaction between the

defective 1MM structure and H_2O was the most favorable, with the lowest interaction energy of -24.25 kcal/mol. The water molecule preferentially interacted with the Zn^{2+} ion at a distance of 2.229 Å, slightly shorter than the 2.840 Å distance to the Cd^{2+} ion.

The second lowest interaction energy was observed for the H_2S molecule, with an energy of -21.49 kcal/mol. The H_2S molecule is positioned near the Cd^{2+} sites at a distance of 2.673 Å, which is longer than the distances between H_2O and Zn^{2+} or Cd^{2+} ions. Following H_2S, CO interacts with the 1MM structure, showing a preferred interaction energy of -11.81 kcal/mol, where the C atom interacts closely with the Zn^{2+} ion at a distance of 2.247 Å. In the case of CO, the carbon atom is closer to the Zn^{2+} ion than the oxygen atom. This can be attributed to the smaller ionic radius of Zn^{2+} compared to Cd^{2+}, resulting in a greater electron attraction to the partially positive C atom of the CO molecule. The next lowest interaction energy is observed for the NO_2 molecule at -9.91 kcal/mol, followed by CO_2 at -7.68 kcal/mol. The trend in interaction energies indicates that favorable interactions generally occur with polar molecules such as H_2O, H_2S, CO, and NO_2.

The interactions of various gas molecules with the defective 2MM structure were also investigated, as shown in Figure 5. Similar to the 1MM structure, the lowest interaction energy was

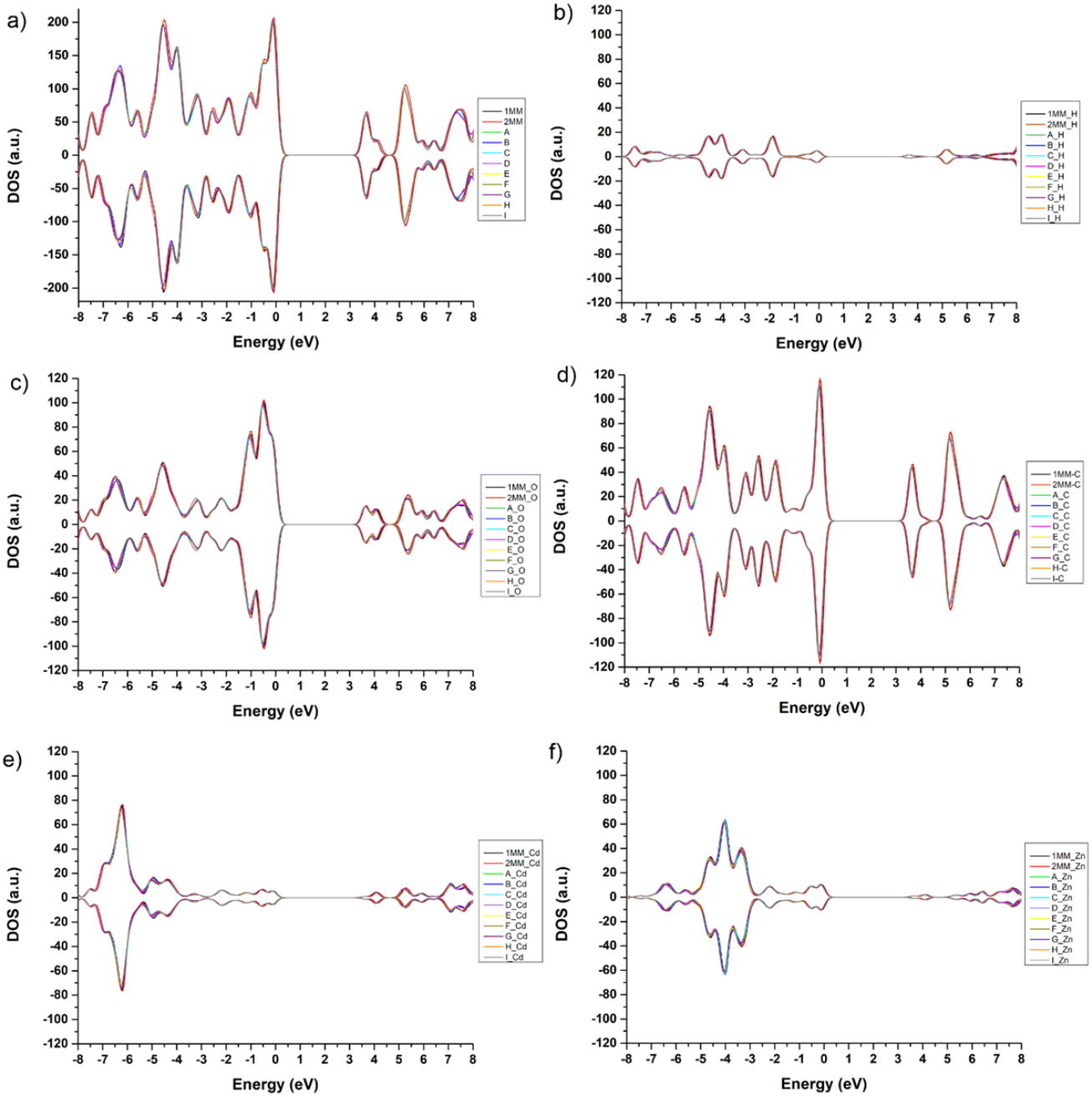

Figure 3. The total DOS (a) as well as partial DOS for each atom (b-f) for non-defective and defective (Zn/Cd)-MOF-5.

observed for the H_2O molecule, with an energy of -24.80 kcal/mol, which is 0.55 kcal/mol lower than the interaction with the 1MM structure. However, the distances between H_2O and the two Cd^{2+} ions are 2.614 Å and 2.626 Å, respectively, which are longer than the distances in the 1MM structure (2.229 Å for Zn^{2+} and 2.840 Å for Cd^{2+}). The next lowest interaction energy was for H_2S, with an energy of -23.55 kcal/mol, which is 2.06 kcal/mol more stable than in the 1MM structure. The distance between S and Zn^{2+} is slightly shorter at 2.663 Å compared to 2.673 Å in the 1MM structure. The interaction energies of NO_2 and CO in the 2MM structure are in the opposite order compared to the 1MM structure. In the 2MM structure, NO_2 has a more stable interaction energy of -12.00 kcal/mol, compared to -10.82 kcal/mol for CO. The stability of NO_2 may be due to the relatively symmetrical distances to both Cd^{2+} ions (2.698 Å and 2.697 Å). In the 1MM structure, the distances between NO_2 and the Cd^{2+} and Zn^{2+} ions are 2.684 Å and 2.439 Å, respectively. The interaction energy of CO_2 is the highest among the tested gases in the 2MM structure, with an energy of -10.42 kcal/mol. Comparing the interactions of CO_2 between the 1MM and 2MM structures, the CO_2 molecule is approximately equidistant from both unsaturated Zn^{2+} and Cd^{2+} ions in the 2MM structure, with distances of 2.712 Å and 2.713 Å, respectively. This equal distance suggests a possible uniform electron density in both regions.

The calculated interaction energies for CO_2 in our defective mixed-metal MOF-5 systems range from -7.68 to -10.42 kcal/mol. To contextualize these values, we compare them with literature data for CO_2 adsorption in various MOFs. Our results align well with the characteristic range for physisorption in MOFs without highly charged, strong Lewis acid metal sites. For instance, the values for other typical MOFs like MOF-808 and Y-CU-10 fall between -0.76 and -1.23 eV (approximately -17.5 to -28.4 kcal/mol) [41].

Notably, our calculated energies are less negative than those reported for MOFs with highly unsaturated, strong Lewis acid metal sites, such as Mg-MOF-74, where values can reach -49.9 kJ/mol (approximately -11.93 kcal/mol) [42] or -

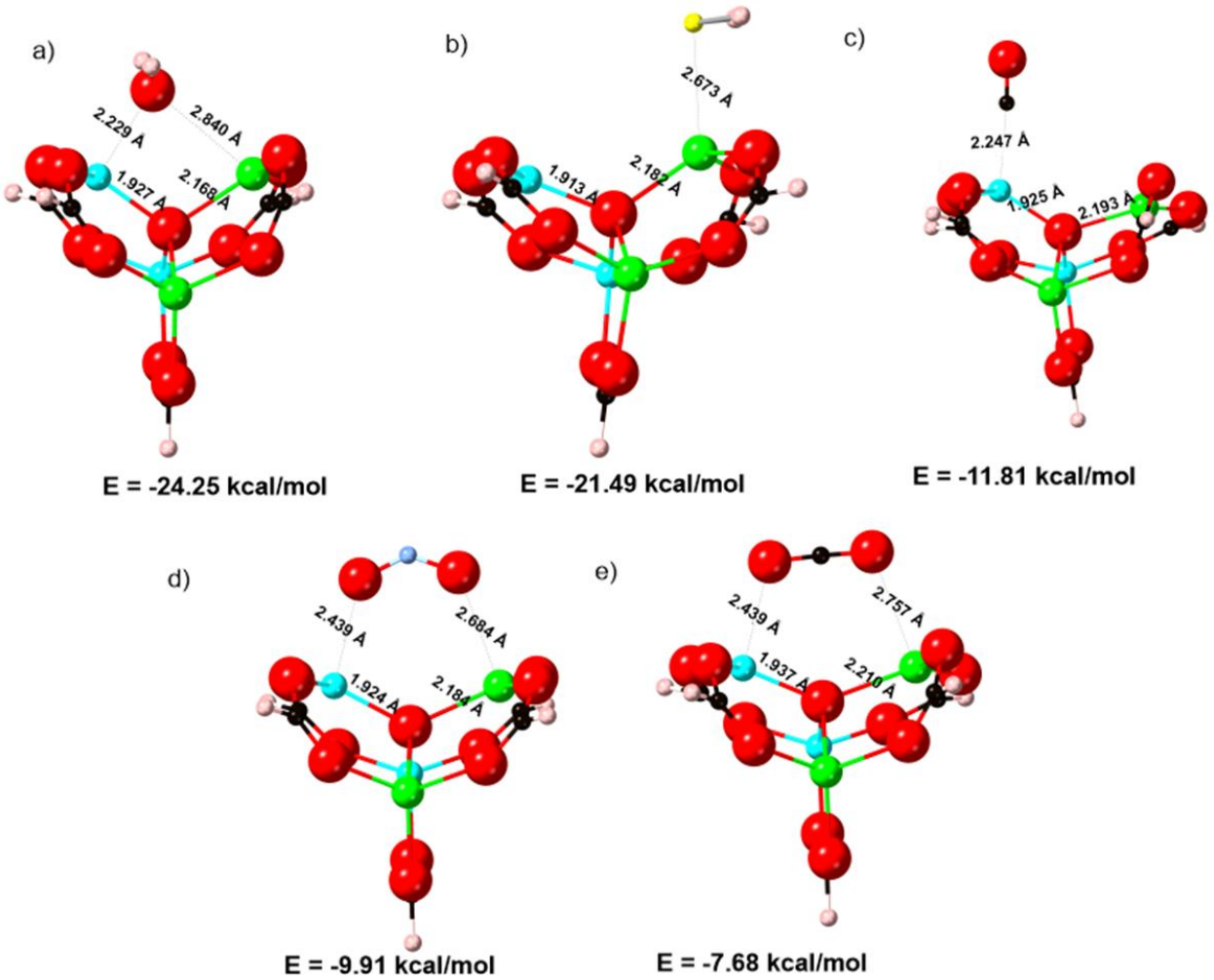

Figure 4. The optimised structures of defective mixed-metal MOF-5 (1MM) in the presence of H_2O (a), H_2S (b), CO (c), NO_2 (d), and CO_2 (e). Zn, Cd, C, O and H are assigned as cyan, green, black, red and pink, respectively.

0.98 eV (approximately -22.6 kcal/mol) [43], which is indicative of stronger chemisorption. This comparison underscores a key characteristic of this system where the defective (Zn/Cd)-MOF-5 provides moderate-affinity binding sites suitable for reversible CO_2 capture. The weaker binding, compared to specialized frameworks like MOF-74, is often advantageous for adsorbent regenerability and energy-efficient cycling, as it requires less energy for CO_2 release. Therefore, the interaction strength observed in these models positions defective mixed-metal MOF-5 as a promising candidate for applications where a balance between adsorption capacity and low regeneration cost is important.

The interaction between polar gas molecules (H_2S, NO_2, H_2O, CO) and defective MOF-5 exhibits more negative adsorption energies compared to non-polar molecules such as CO_2. This suggests that prolonged exposure of MOF-5 to polar gases could lead to structural instability in the framework. Previous studies have reported that polar gas molecules induce structural collapse in various MOFs due to their stronger interactions with the inorganic nodes, which disrupt the coordination bonds critical to the framework integrity [44–46]. In contrast, CO_2 demonstrates the least negative binding energy among the tested gases, indicative of weaker intermolecular interactions with the MOF-5 framework. This weaker interaction may reduce framework degradation and enhance recyclability, making CO_2 a more viable candidate for gas capture applications in defective MOF-5 systems.

Among the studied gas molecules, H_2O exhibits the most favorable interaction energy with both 1MM and 2MM structures. The exceptionally strong adsorption of water molecules (-24.25 to -24.80 kcal/mol) on the defective mixed-metal MOF-5 has profound implications for its stability and practical application, particularly in humid environments. This strong interaction energy, which is

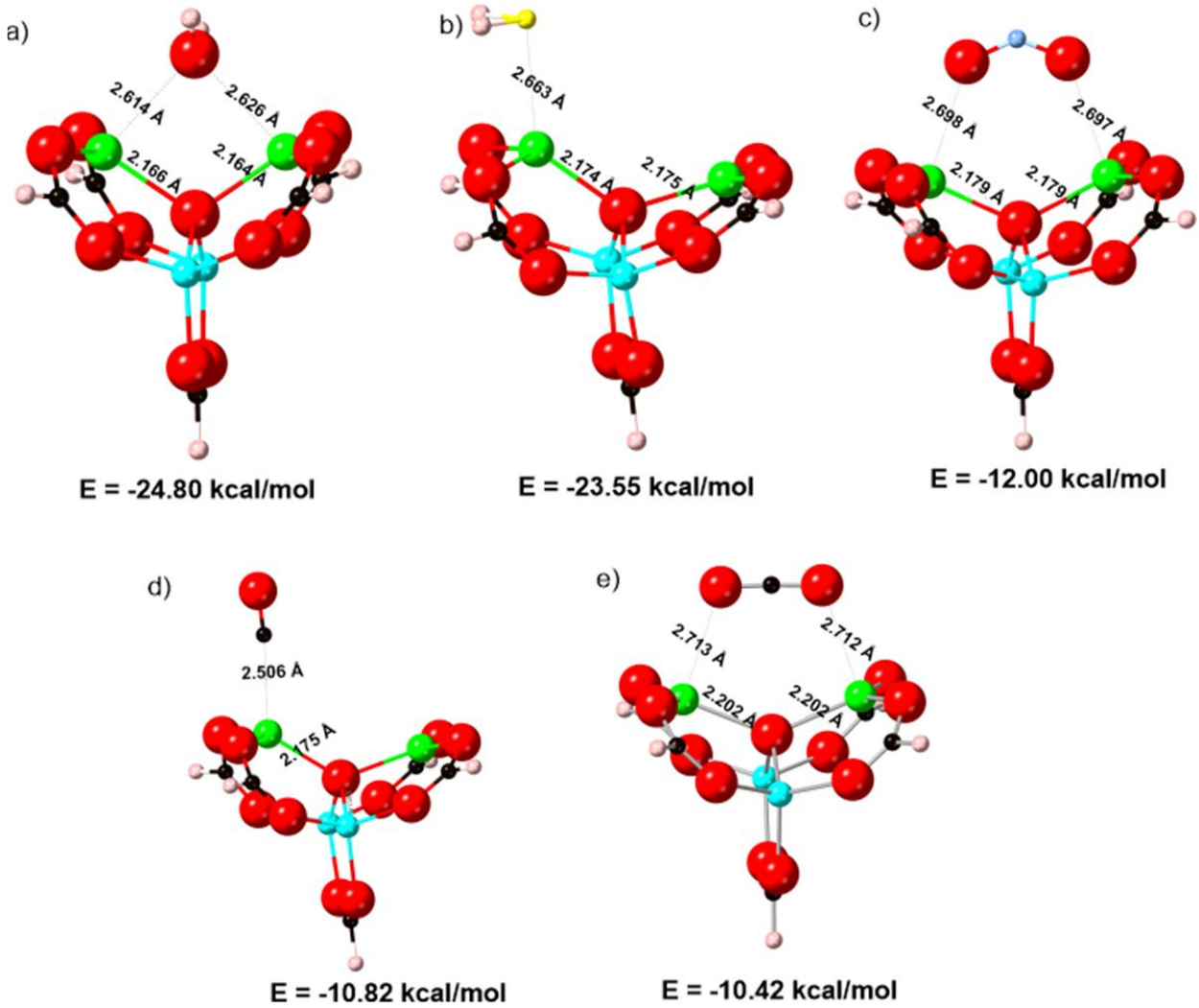

Figure 5. The optimised structures of defective mixed-metal (Zn/Cd)-MOF-5 (2MM) in the presence of H_2O (a), H_2S (b), NO_2 (c), CO (d), and CO_2 (e). Zn, Cd, C, O and H are assigned as cyan, green, black, red and pink, respectively.

characteristic of a robust chemisorption process, suggests that water is not merely physisorbed but forms a strong coordinative bond with the unsaturated metal sites created by the missing linker defects. This finding raises a concern regarding the hydrostability of the framework. It is well-established that pristine Zn-MOF-5 is susceptible to structural degradation in the presence of water, a process often initiated by the displacement of the organic linker (bdc^{2-}) by H_2O molecules, which attack the Zn-O clusters [47–49]. Our results indicate that the introduction of defects exacerbates this vulnerability. The unsaturated Zn^{2+} and Cd^{2+} sites in the defective structures act as primary targets for water molecules, providing a low-energy pathway for water to infiltrate and attack the inorganic node.

To evaluate this phenomenon, we conducted a visual study of weak interactions between H_2O and the 1MM or 2MM structures, as shown in Figures 6a and 6b. We used the independent gradient model based on the Hirshfeld method (IGMH) to differentiate between possible weak and strong interactions [50]. In Figure 6, the blue

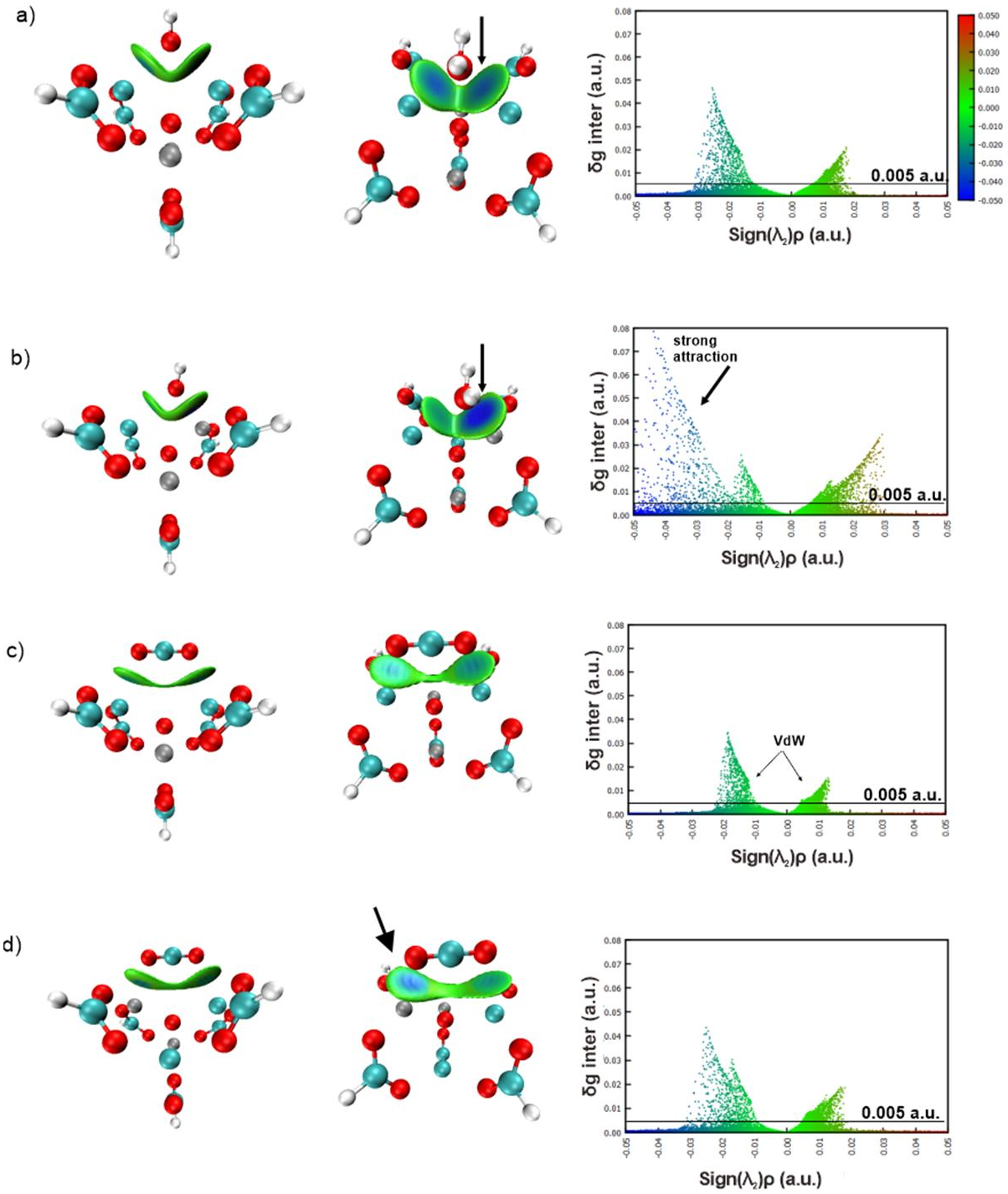

Figure 6. The interaction of H_2O with 2MM(a) and 1MM (b) as well as CO_2 with 2MM (c) and 1MM (d). The isosurface map in different orientation is shown together with the IGMH plot.

region where $sign(\lambda_2)\rho < 0.02$ au indicates possible strong interactions between the components under study. The green region, with $-0.02 < sign(\lambda_2)\rho < 0.02$, indicates possible weak interactions, such as van der Waals attractions.

In Figure 6a, the interaction of H_2O with the 2MM structure results in an interaction energy of -24.80 kcal/mol, with a combination of strong and weak interactions as shown in the isosurface map. The green isosurface dominates, indicating van der Waals interactions. However, a closer look at the isosurface maps and the IGMH plot reveals possible strong attractions, indicated by the blue region. This strong interaction is likely due to the interaction between the oxygen of the H_2O molecule and the Cd^{2+} ions. Since the distances between H_2O and the two Cd^{2+} ions are relatively similar, the distribution of the strong attraction region is also similar.

In contrast, Figure 6b shows a different behavior for H_2O in the 1MM structure, where the strong attraction region is larger when the oxygen atom of H_2O interacts with the Zn^{2+} ion. This strong attraction explains the shorter distance of H_2O to Zn^{2+} (2.229 Å) compared to Cd^{2+} (2.840 Å). The presence of strong attractions in both the 1MM and 2MM structures may explain why the water molecule has a greater tendency to interact with defective (Zn/Cd)-MOF-5.

The interaction modes between CO_2 and both the 2MM and 1MM structures are shown in Figures 6c and 6d, respectively. CO_2 exhibits the highest (least negative) interaction energy among the small molecules studied. As shown in the isosurface map, weak interactions, likely van der Waals interactions, dominate, as indicated by the $-0.02 < sign(\lambda_2)\rho < 0.02$ range in the IGMH plot. This may explain why CO_2 has a lower preference for interaction compared to H_2O, H_2S, NO_2, and CO. Additionally, the non-polar nature of CO_2 is more apparent compared to the other gas molecules in this study. However, CO_2 interacting with the 1MM structure (Figure 6d) shows an indication of strong attraction with a small blue region, due to the close interaction between the oxygen of CO_2 and the Zn^{2+} ion at 2.439 Å.

The single-molecule adsorption energies reported here provide fundamental insight into the intrinsic affinity of the defective sites for various gases. Building on these results, future work may involve Grand Canonical Monte Carlo (GCMC) simulations to predict multicomponent adsorption isotherms and selectivity, such as for CO_2/H_2O mixtures, which is essential for evaluating the practical potential of these defective mixed-metal MOFs in industrial gas separation processes. The computational insights presented here also provide a strong foundation for subsequent experimental validation. Future work may focus on the synthesis of these mixed-metal and defective MOF-5 variants, guided by the structural parameters and stability trends predicted in this study.

4. Conclusion

The formation of missing linker defects in (Zn/Cd)-MOF-5 has been thoroughly investigated in terms of structural characteristics, electronic properties, and interactions with various small gas molecules. The absence of one bdc^{2-} linker slightly affects the unit cell dimensions, particularly in the direction of the bdc^{2-} removal along the b-lattice. The electronic properties of the missing linker defect were assessed based on bandgap energy and DOS profiles. The bandgap energy slightly decreases when a bdc^{2-} linker is removed from (Zn/Cd)-MOF-5, as indicated by minor differences in the electronic states of C and O at the edges of both the valence and conduction bands. The reaction energy of the missing linker defect is positive, indicating it is relatively unfavorable, with values ranging from 0.24 to 0.60 eV. The preferred location for bdc^{2-} linker removal is generally where Zn^{2+} and Cd^{2+} ions are initially attached. However, the reaction energy is relatively high when the bdc^{2-} linker is initially attached to both Cd^{2+} ions. The potential application of defective (Zn/Cd)-MOF-5 for gas adsorption was studied for various gas molecules, including CO_2, H_2S, H_2O, CO, and NO_2. In general, the interactions are favorable, with negative binding energies for all gas molecules, and H_2O showing the most negative value. The interaction energy of CO_2 is the least negative compared to other gas molecules, indicating a possible pathway for gas separation. The preferred interaction modes were studied using the independent gradient model based on Hirshfeld partitioning, indicating possible strong or weak interactions between gas molecules and defect structures. Favorable gas molecule interactions are indicated by the presence of strong attractions combined with weak interactions, such as van der Waals forces. This study provides an in-depth analysis of the structure, electronic properties, and gas adsorption applications in the development of defective mixed-metal MOFs.

Acknowledgment

The authors greatly thanks to the research grant provided by Universitas Gadjah Mada through the Academic Excellence Program Scheme B with the contract number of 4419/UN1/DITLIT/PT.01.03/2024.

CRedit Author Statement

Author Contributions: Fajar. I Pambudi: Conceptualization, Methodology, Validation, Formal analysis, Investigation, Writing – original draft, Eko Sri Kunarti: Validation, Writing – review & editing, Robby Noor Cahyono: Validation, Writing – review & editing, Nabila Nur Agusti: Validation, Investigation, Writing – review & editing. The authors have read and agreed to the published version of the manuscript.

References

[1] Kirchon, A., Feng, L., Drake, H.F., Joseph, E.A., Zhou, H.-C. (2018). From fundamentals to applications: a toolbox for robust and multifunctional MOF materials. *Chemical Society Reviews*, 47(23), 8611–8638. DOI: 10.1039/C8CS00688A.

[2] Fonseca, J., Gong, T., Jiao, L., Jiang, H.-L. (2021). Metal–organic frameworks (MOFs) beyond crystallinity: amorphous MOFs, MOF liquids and MOF glasses. *Journal of Materials Chemistry A*, 9(17), 10562–10611. DOI: 10.1039/D1TA01043C.

[3] Stock, N., Biswas, S. (2012). Synthesis of metal-organic frameworks (MOFs): Routes to various MOF topologies, morphologies, and composites. *Chemical Reviews*, 112(2), 933–969. DOI: 10.1021/cr200304e.

[4] Liu, C., Wang, J., Wan, J., Yu, C. (2021). MOF-on-MOF hybrids: Synthesis and applications. *Coordination Chemistry Reviews*, 432, 213743. DOI: 10.1016/j.ccr.2020.213743.

[5] Ding, M., Flaig, R.W., Jiang, H.-L., Yaghi, O.M. (2019). Carbon capture and conversion using metal–organic frameworks and MOF-based materials. *Chemical Society Reviews*, 48(10), 2783–2828. DOI: 10.1039/C8CS00829A.

[6] Wang, Q., Astruc, D. (2020). State of the Art and Prospects in Metal–Organic Framework (MOF)-Based and MOF-Derived Nanocatalysis. *Chemical Reviews*, 120(2), 1438–1511. DOI: 10.1021/acs.chemrev.9b00223.

[7] Shi, Y., Yang, A.F., Cao, C.S., Zhao, B. (2019). Applications of MOFs: Recent advances in photocatalytic hydrogen production from water. *Coordination Chemistry Reviews*, 390, 50–75. DOI: 10.1016/j.ccr.2019.03.012.

[8] Freund, R., Zaremba, O., Arnauts, G., Ameloot, R., Skorupskii, G., Dincă, M., Bavykina, A., Gascon, J., Ejsmont, A., Goscianska, J., Kalmutzki, M., Lächelt, U., Ploetz, E., Diercks, C.S., Wuttke, S. (2021). The Current Status of MOF and COF Applications. *Angewandte Chemie International Edition*, 60(45), 23975–24001. DOI: 10.1002/anie.202106259.

[9] Yusuf, V.F., Malek, N.I., Kailasa, S.K. (2022). Review on Metal-Organic Framework Classification, Synthetic Approaches, and Influencing Factors: Applications in Energy, Drug Delivery, and Wastewater Treatment. *ACS Omega*, 7(49), 44507–44531. DOI: 10.1021/acsomega.2c05310.

[10] Srepusharawoot, P., Araújo, C.M., Blomqvist, A., Scheicher, R.H., Ahuja, R. (2008). A comparative investigation of H2 adsorption strength in Cd- and Zn-based metal organic framework-5. The *Journal of Chemical Physics*, 129(16) DOI: 10.1063/1.2997377.

[11] EL Kassaoui, M., Lakhal, M., Benyoussef, A., El Kenz, A., Loulidi, M. (2021). Enhancement of hydrogen storage properties of metal-organic framework-5 by substitution (Zn, Cd and Mg) and decoration (Li, Be and Na). *International Journal of Hydrogen Energy*, 46(52), 26426–26436. DOI: 10.1016/j.ijhydene.2021.05.107.

[12] Denny, M.S., Kalaj, M., Bentz, K.C., Cohen, S.M. (2018). Multicomponent metal-organic framework membranes for advanced functional composites. *Chemical Science*, 9(47), 8842–8849. DOI: 10.1039/c8sc02356e.

[13] Bae, Y.-S., Mulfort, K.L., Frost, H., Ryan, P., Punnathanam, S., Broadbelt, L.J., Hupp, J.T., Snurr, R.Q. (2008). Separation of CO2 from CH 4 Using Mixed-Ligand Metal−Organic Frameworks. *Langmuir*, 24(16), 8592–8598. DOI: 10.1021/la800555x.

[14] Marti, R.M., Howe, J.D., Morelock, C.R., Conradi, M.S., Walton, K.S., Sholl, D.S., Hayes, S.E. (2017). CO2 dynamics in pure and mixed-metal MOFs with open metal sites. *Journal of Physical Chemistry C*, 121(39) DOI: 10.1021/acs.jpcc.7b07179.

[15] Sun, D., Sun, F., Deng, X., Li, Z. (2015). Mixed-Metal Strategy on Metal-Organic Frameworks (MOFs) for Functionalities Expansion: Co Substitution Induces Aerobic Oxidation of Cyclohexene over Inactive Ni-MOF-74. *Inorganic Chemistry*, 54(17), 8639–8643. DOI: 10.1021/acs.inorgchem.5b01278.

[16] Pambudi, F.I. (2022). Electronic properties of heterometallic zeolitic imidazolate framework and its encapsulation with Ni, Pd and Pt. *Inorganic Chemistry Communications*, 143, 109798. DOI: 10.1016/j.inoche.2022.109798.

[17] Zhang, S., Liu, J., Liu, L. (2021). Insights into the thermal conductivity of MOF-5 from first principles. *RSC Advances*, 11(58), 36928–36933. DOI: 10.1039/D1RA07022C.

[18] Mali, G., Mazaj, M., Arčon, I., Hanžel, D., Arčon, D., Jagličić, Z. (2019). Unraveling the Arrangement of Al and Fe within the Framework Explains the Magnetism of Mixed-Metal MIL-100(Al,Fe). *Journal of Physical Chemistry Letters*, 10(7), 1464–1470. DOI: 10.1021/acs.jpclett.9b00341.

[19] Sun, J., Semenchenko, L., Lim, W.T., Ballesteros Rivas, M.F., Varela-Guerrero, V., Jeong, H.K. (2018). Facile synthesis of Cd-substituted zeolitic-imidazolate framework Cd-ZIF-8 and mixed-metal CdZn-ZIF-8. *Microporous and Mesoporous Materials*, 264, 35–42. DOI: 10.1016/j.micromeso.2017.12.032.

[20] Lomachenko, K.A., Jacobsen, J., Bugaev, A.L., Atzori, C., Bonino, F., Bordiga, S., Stock, N., Lamberti, C. (2018). Exact Stoichiometry of Ce x Zr 6-x Cornerstones in Mixed-Metal UiO-66 Metal-Organic Frameworks Revealed by Extended X-ray Absorption Fine Structure Spectroscopy. *Journal of the American Chemical Society*, 140(50), 17379–17383. DOI: 10.1021/jacs.8b10343.

[21] Tang, J., Li, S., Xu, J., Deng, F. (2022). Spectroscopic Characterizations of Porous Mixed Metal Oxides Derived from Metal–Organic Framework MIL-53(Ga, Al) for Propane Dehydrogenation. *The Journal of Physical Chemistry C*, 126(31), 13485–13495. DOI: 10.1021/acs.jpcc.2c04072.

[22] Jia, H., Han, Q., Luo, W., Cong, H., Deng, H. (2022). Sequence control of metals in MOF by coordination number precoding for electrocatalytic oxygen evolution. *Chem Catalysis*, 2(1), 84–101. DOI: 10.1016/j.checat.2021.10.007.

[23] Fang, Z., Bueken, B., De Vos, D.E., Fischer, R.A. (2015). Defect-Engineered Metal-Organic Frameworks. *Angewandte Chemie - International Edition*, 54(25), 7234–7254. DOI: 10.1002/anie.201411540.

[24] Cai, G., Jiang, H.L. (2017). A Modulator-Induced Defect-Formation Strategy to Hierarchically Porous Metal–Organic Frameworks with High Stability. *Angewandte Chemie International Edition*, 56(2), 563–567. DOI: 10.1002/anie.201610914.

[25] Xiang, W., Zhang, Y., Chen, Y., Liu, C.J., Tu, X. (2020). Synthesis, characterization and application of defective metal-organic frameworks: Current status and perspectives. *Journal of Materials Chemistry A*, 8(41), 21526–21546. DOI: 10.1039/d0ta08009h.

[26] Feng, Y., Chen, Q., Jiang, M., Yao, J. (2019). Tailoring the Properties of UiO-66 through Defect Engineering: A Review. *Industrial and Engineering Chemistry Research*, 58(38), 17646–17659. DOI: 10.1021/acs.iecr.9b03188.

[27] Hou, X., Wang, J., Mousavi, B., Klomkliang, N., Chaemchuen, S. (2022). Strategies for induced defects in metal–organic frameworks for enhancing adsorption and catalytic performance. *Dalton Transactions*, 51(21), 8133–8159. DOI: 10.1039/D2DT01030E.

[28] Portillo-Vélez, N.S., Obeso, J.L., de los Reyes, J.A., Peralta, R.A., Ibarra, I.A., Huxley, M.T. (2024). Benefits and complexity of defects in metal-organic frameworks. *Communications Materials*, 5(1), 247. DOI: 10.1038/s43246-024-00691-1.

[29] Mautschke, H.H., Drache, F., Senkovska, I., Kaskel, S., Llabrés Xamena, F.X.I. (2018). Catalytic properties of pristine and defect-engineered Zr-MOF-808 metal organic frameworks. *Catalysis Science & Technology*, 8(14), 3610–3616. DOI: 10.1039/C8CY00742J.

[30] Cheng, P., Hu, Y.H. (2016). Acetylene adsorption on defected MIL-53. *International Journal of Energy Research*, 40(6), 846–852. DOI: 10.1002/ER.3492.

[31] Ardila-Suárez, C., Perez-Beltran, S., Ramírez-Caballero, G.E., Balbuena, P.B. (2018). Enhanced acidity of defective MOF-808: effects of the activation process and missing linker defects. *Catalysis Science & Technology*, 8(3), 847–857. DOI: 10.1039/C7CY02462B.

[32] Iacomi, P., Formalik, F., Marreiros, J., Shang, J., Rogacka, J., Mohmeyer, A., Behrens, P., Ameloot, R., Kuchta, B., Llewellyn, P.L. (2019). Role of Structural Defects in the Adsorption and Separation of C3 Hydrocarbons in Zr-Fumarate-MOF (MOF-801). *Chemistry of Materials*, 31(20), 8413–8423. DOI: 10.1021/acs.chemmater.9b02322.

[33] Prasetya, N., Li, K. (2022). Synthesis of defective MOF-801 via an environmentally benign approach for diclofenac removal from water streams. *Separation and Purification Technology*, 301, 122024. DOI: 10.1016/j.seppur.2022.122024.

[34] Zoundi, Z. (2017). CO2 emissions, renewable energy and the Environmental Kuznets Curve, a panel cointegration approach. *Renewable and Sustainable Energy Reviews*, 72, 1067–1075. DOI: 10.1016/j.rser.2016.10.018.

[35] Eddaoudi, M., Li, H., Reineke, T., Fehr, M., Kelley, D., Groy, T.L., Yaghi, O.M. (1999). Design and synthesis of metal-carboxylate frameworks with permanent microporosity. *Topics in Catalysis*, 9(1/2), 105–111. DOI: 10.1023/A:1019110622091.

[36] Kühne, T.D., Iannuzzi, M., Del Ben, M., Rybkin, V. V., Seewald, P., Stein, F., Laino, T., Khaliullin, R.Z., Schütt, O., Schiffmann, F., Golze, D., Wilhelm, J., Chulkov, S., Bani-Hashemian, M.H., Weber, V., Borštnik, U., Taillefumier, M., Jakobovits, A.S., Lazzaro, A., Pabst, H., Müller, T., Schade, R., Guidon, M., Andermatt, S., Holmberg, N., Schenter, G.K., Hehn, A., Bussy, A., Belleflamme, F., Tabacchi, G., Glöß, A., Lass, M., Bethune, I., Mundy, C.J., Plessl, C., Watkins, M., VandeVondele, J., Krack, M., Hutter, J. (2020). CP2K: An electronic structure and molecular dynamics software package - Quickstep: Efficient and accurate electronic structure calculations. *The Journal of Chemical Physics*, 152(19) DOI: 10.1063/5.0007045.

[37] Neese, F. (2012). The ORCA program system. Wiley Interdisciplinary Reviews: Computational Molecular Science, 2(1), 73–78. DOI: 10.1002/WCMS.81.

[38] Yang, L.-M., Fang, G.-Y., Ma, J., Ganz, E., Han, S.S. (2014). Band Gap Engineering of Paradigm MOF-5. *Crystal Growth & Design*, 14(5), 2532–2541. DOI: 10.1021/cg500243s.

[39] Pambudi, F.I., Prasetyo, N. (2021). Theoretical investigation on the structure of mixed-metal zeolitic imidazolate framework and its interaction with CO2. *Computational Materials Science*, 111033. DOI: 10.1016/j.commatsci.2021.111033.

[40] Pambudi, F.I., Pratiwi, N.S., Chusnawati, U. (2023). First-principle study on the lattice-directed missing linker defect in zirconium based metal-organic framework (MOF-801): Electronic properties and interaction with hydrogen. *Materials Today Communications*, 35, 105967. DOI: 10.1016/j.mtcomm.2023.105967.

[41] Tassé, D., Quezada-Novoa, V., Copeman, C., Howarth, A.J., Rochefort, A. (2025). Identification of Adsorption Sites for CO2 in a Series of Rare-Earth and Zr-Based Metal-Organic Frameworks. *ChemPhysChem*, 26(10) DOI: 10.1002/cphc.202401050.

[42] Yu, J., Balbuena, P.B. (2013). Water Effects on Postcombustion CO2 Capture in Mg-MOF-74. *The Journal of Physical Chemistry C*, 117(7), 3383–3388. DOI: 10.1021/jp311118x.

[43] Nachimuthu, S., Su, M.-S., Wu, L.-T., Yu, C.-T., Jiang, J.-C. (2025). Tunable CO2 capture in N-ethylethylenediamine functionalized Mg2-MOF-74: unraveling the role of diamine basicity in reactivity and adsorption capacity. *Chemical Engineering Journal*, 515, 163587. DOI: 10.1016/j.cej.2025.163587.

[44] Martínez-Ahumada, E., López-Olvera, A., Jancik, V., Sánchez-Bautista, J.E., González-Zamora, E., Martis, V., Williams, D.R., Ibarra, I.A. (2020). MOF Materials for the Capture of Highly Toxic H2S and SO2. *Organometallics*, 39(7), 883–915. DOI: 10.1021/acs.organomet.9b00735.

[45] Hamon, L., Serre, C., Devic, T., Loiseau, T., Millange, F., Férey, G., Weireld, G. De (2009). Comparative Study of Hydrogen Sulfide Adsorption in the MIL-53(Al, Cr, Fe), MIL-47(V), MIL-100(Cr), and MIL-101(Cr) Metal−Organic Frameworks at Room Temperature. *Journal of the American Chemical Society*, 131(25), 8775–8777. DOI: 10.1021/ja901587t.

[46] Petit, C., Mendoza, B., Bandosz, T.J. (2010). Hydrogen Sulfide Adsorption on MOFs and MOF/Graphite Oxide Composites. *ChemPhysChem*, 11(17), 3678–3684. DOI: 10.1002/cphc.201000689.

[47] An, Y., Lv, X., Jiang, W., Wang, L., Shi, Y., Hang, X., Pang, H. (2024). The stability of MOFs in aqueous solutions—research progress and prospects. *Green Chemical Engineering*, 5(2), 187–204. DOI: 10.1016/j.gce.2023.07.004.

[48] Ming, Y., Kumar, N., Siegel, D.J. (2017). Water Adsorption and Insertion in MOF-5. *ACS Omega*, 2(8), 4921–4928. DOI: 10.1021/acsomega.7b01129.

[49] Qi, Z.-P., Yang, J.-M., Kang, Y.-S., Guo, F., Sun, W.-Y. (2016). Facile water-stability evaluation of metal–organic frameworks and the property of selective removal of dyes from aqueous solution. *Dalton Transactions*, 45(21), 8753–8759. DOI: 10.1039/C6DT00886K.

[50] Lu, T., Chen, Q. (2022). Independent gradient model based on Hirshfeld partition: A new method for visual study of interactions in chemical systems. *Journal of Computational Chemistry*, 43(8), 539–555. DOI: 10.1002/jcc.26812.